PCCP

PAPER

View Article Online
View Journal | View Issue

Cite this: *Phys. Chem. Chem. Phys.*, 2014, **16**, 5412

An oxygen evolution Co–Ac catalyst – the synergistic effect of phosphate ions†

Ahamed Irshad and Nookala Munichandraiah*

Received 18th November 2013,
Accepted 19th January 2014

DOI: 10.1039/c3cp54860k

www.rsc.org/pccp

Formation of an amorphous cobalt based oxygen evolution catalyst called Co–Pi has been recently reported from a neutral phosphate buffer solution containing Co^{2+}. But the concentration of Co^{2+} is as low as 0.5 mM due to poor solubility of a cobalt salt in phosphate medium. In the present study, a cobalt acetate based oxygen evolution catalyst (Co–Ac) is prepared from a neutral acetate buffer solution, where the solubility of Co^{2+} is very high (>100 times in comparison with phosphate buffer solution). The Co–Ac possesses better catalytic activity than the Co–Pi with an additional advantage of easy bulk scale preparation. The comparative studies on the oxygen evolution reaction (OER) activity of Co–Ac and Co–Pi in phosphate and acetate buffer electrolytes reveal that the Co–Ac exhibits enhanced synergistic catalytic activity in phosphate solution, probably due to partial substitution of acetate in the catalyst layer by phosphate, resulting in the formation of a Co–Ac–Pi catalyst.

1. Introduction

The global energy demand has increased considerably in recent years owing to an increase in human population and industrialization. The energy demand is met primarily by burning fossil fuels, which are non-renewable and also cause serious environmental problems.[1–3] Hence, exploration of appropriate renewable energy sources as alternatives for the conventional fossil fuels is one of the scientific challenges of the present century. Among the renewable energy sources, solar energy has enormous potential to meet the future energy needs. Since it is diurnal, utilization of solar energy requires a suitable means of its storage.[4,5] Photoassisted electrolysis of water is one of the promising methods for solar energy storage.[6,7] The process involves oxidation of water to oxygen and reduction of protons to hydrogen. The produced hydrogen gas can be stored as a fuel for energy conversion in the absence of solar radiation. The efficiency of electrolysis of water is mainly limited by the complex multistep and multi-electron oxygen evolution reaction.[8–10] Hence, the design of an efficient and cost effective oxygen evolution reaction (OER) catalyst is a challenging task in solar energy storage.

Formation of an amorphous cobalt based oxygen evolution catalyst (OEC), namely, Co–Pi has been reported in recent years.[11] The catalyst is very promising owing to its high catalytic activity, easy formation and self-repairing property.[11,12] The catalyst functions in neutral electrolytes with moderate overpotentials for OER. Interfacing of Co–Pi with various semiconducting materials such as Si,[13] ZnO,[14] TiO_2,[15] WO_3,[16] α-Fe_2O_3[17–19] and $BiVO_4$[20] is also reported for photoelectrolysis of water. However, the chemical composition of the catalyst, role of phosphate in catalysis and mechanism of OER are not well understood.[21,22] Furthermore, formation of thick layers of a Co–Pi catalyst prior to water electrolysis is a tedious and time consuming process owing to poor solubility of Co^{2+} salts in neutral phosphate buffer solution. Until now, most of the studies reported on Co–Pi catalysts employed phosphate buffer solutions of pH $\sim$ 7.0 with a Co^{2+} salt concentration of 0.5 mM. At this concentration, the solution reaches saturation with respect to the Co^{2+} ion. Therefore, there is a need for the demonstration of catalysts in alternate buffer solutions in which Co^{2+} salts can be dissolved at high concentrations. A high concentration of Co^{2+} is an advantage because the rate of electrodeposition can be enhanced and also thicker layers of the catalyst can be deposited in a short time.

In the present study, electrochemical deposition of a cobalt acetate based oxygen evolution catalyst (Co–Ac) from a neutral acetate buffer solution containing a high concentration of Co^{2+} is reported. The Co–Ac catalyst is more efficient than Co–Pi under similar experimental conditions. Comparative studies on the OER activity of Co–Ac and Co–Pi catalysts in phosphate and acetate buffer electrolytes reveal that there is a synergistic effect of phosphate and acetate ions on the OER activity of Co–Ac and Co–Pi catalysts, respectively.

2. Experimental methods

Analytical grade $Co(NO_3)_2{\cdot}6H_2O$, glacial acetic acid (S.D. Fine Chemicals), CH_3COONa, KH_2PO_4 (Merck) and K_2HPO_4 (Merck)

Department of Inorganic and Physical Chemistry Indian Institute of Science, Bangalore - 560012, India. E-mail: muni@ipc.iisc.ernet.in; Tel: +91-80-2293 3183

† Electronic supplementary information (ESI) available. See DOI: 10.1039/c3cp54860k

were used as received. All solutions were prepared in doubly distilled water. Phosphate buffer solution was prepared by titrating 0.1 M KH_2PO_4 solution against 0.1 M K_2HPO_4 solution. Similarly, acetate buffer solution was prepared by mixing 0.1 M CH_3COONa and 0.1 M glacial acetic acid solutions. The pH of buffer solutions was 7.0, unless otherwise stated. A Toray carbon paper of thickness 0.2 mm was used as the working electrode for electrochemical measurements. A section of 7 mm width and 3 cm length was cut from a carbon paper sheet and 1.4 cm^2 area was exposed to the electrolyte. The rest of its length was used for electrical contact through a Cu wire. The unexposed area of the electrode was masked by a PTFE tape. Pt foil auxiliary electrodes and saturated calomel reference electrode (SCE) were used in a glass cell. Microscopic analysis was carried out by using a FEI Company scanning electron microscope (SEM) model SIRION equipped with an EDX system at an accelerating voltage of 10 kV. For EDXA analysis, catalyst film was electrodeposited on an indium tin oxide (ITO) coated glass electrode instead of carbon paper. The surface chemistry of catalyst film was examined by X-ray photoelectron spectroscopy (XPS) using a SPECS GmbH spectrometer (Phoibos100MCD Energy Analyzer) with Mg Kα radiation (1253.6 eV). The peak of C1s at 284.6 eV was taken as the reference energy position. Infrared spectroscopy measurements were recorded in a range of 400 to 4000 cm^{-1} using a JASCO FT/IR-4000 model. Samples were dried well and diluted by KBr. Powder X-ray diffraction (XRD) patterns were collected using a Bruker D8 diffractometer and using Cu Kα radiation. Electrochemical experiments were carried out using a PARC EG&G potentiostat/galvanostat model Versastat II. Mass variations during various electrochemical experiments were monitored using a CH Instruments potentiostat/galvanostat model 440A equipped with an electrochemical quartz crystal microbalance (EQCM). A Teflon cell of about 10 ml capacity with an Au-coated quartz crystal (8 MHz, active area – 0.205 cm^2, sensitivity – 0.146 Hz ng^{-1} cm^2) working electrode, Ag/AgCl, a 3 M KCl reference electrode and a Pt wire counter electrode was used. All potential values are converted and reported against normal hydrogen electrode (NHE) reference. Current density values are reported on the basis of geometrical area of the electrode. All electrochemical experiments were performed at 22 ± 1 °C.

3. Results and discussion

3.1 Co–Ac formation and the effect of Co^{2+} concentration

Cyclic voltammograms of carbon paper electrodes in 0.1 M acetate and 0.1 M phosphate buffer (pH 7.0) solutions in the absence and presence of 0.5 mM Co^{2+} are shown in Fig. 1. The voltammogram in 0.1 M phosphate buffer solution containing 0.5 mM Co^{2+} (Fig. 1 curve i) shows a broad current peak at 1.10 V corresponding to the oxidation of Co^{2+} to Co^{3+} and subsequent formation of the Co–Pi catalyst similar to the results reported on the fluorine doped indium tin oxide (FTO) electrode.[11] This is followed by a large increase in the current due to the oxidation of water to produce oxygen. To investigate

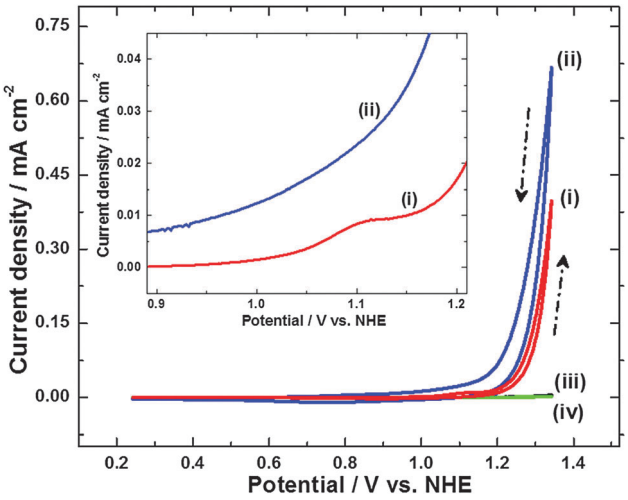

Fig. 1 Cyclic voltammograms of the carbon paper electrode in (i) 0.1 M phosphate solution containing 0.5 mM Co^{2+}, (ii) 0.1 M acetate solution containing 0.5 mM Co^{2+}, (iii) 0.1 M acetate solution without Co^{2+} and (iv) 0.1 M phosphate solution without Co^{2+}. pH of the solutions = 7.0. The inset shows the enlarged region of the Co^{2+} oxidation peak. Sweep rate: 5 mV s^{-1}.

a similar phenomenon in acetate buffer solution, cyclic voltammetry experiments were carried out (Fig. 1 curve ii) in 0.5 mM Co^{2+} + 0.1 M acetate buffer solution of pH 7.0. Although, the voltammogram does not exhibit any current peak corresponding to Co^{2+} oxidation (inset in Fig. 1 curve ii), a relatively more intense anodic wave for water oxidation is observed, suggesting the electrodeposition of a more efficient Co–Ac catalyst than Co–Pi prior to the onset of OER. To examine a possible decomposition of the acetate ion in this potential range, experiments were repeated with 0.1 M acetate buffer solution without the Co^{2+} salt (Fig. 1 curve iii). The voltammogram is quite similar to the one recorded in phosphate buffer solution (Fig. 1 curve iv), suggesting the absence of acetate oxidation in this potential range. In the absence of Co^{2+} ions in acetate and phosphate solutions (Fig. 1 curves iii and iv), negligibly small current flows through the carbon paper electrodes. To further confirm the electrochemical stability of the acetate ion, a Pt foil electrode was cycled in acetate buffer solution (ESI,† Fig. S1). When cycled between 0.20 and 1.50 V, current increased at about 1.40 V due to OER. There was no indication of oxidation of acetate. Thus, the large magnitude of current observed in the presence of Co^{2+} (Fig. 1 curves i and ii) is due to the catalytic effect of the electrodeposits. The values of current density at 1.34 V are 0.66 and 0.40 mA cm^{-2}, respectively, in acetate and phosphate electrolytes. As the magnitude of current at 1.34 V is greater in acetate solution than the corresponding values in phosphate solution, it is inferred that the Co–Ac is a better catalyst than Co–Pi for OER. Similar to the present studies on preparation of the Co-based OER catalyst from acetate electrolytes, the Mn-based catalyst was prepared from acetate electrolytes.[23] Furthermore, the gas evolution from the Co–Ac catalyst was identified by subjecting a Pt foil electrode introduced into the electrochemical cell to linear

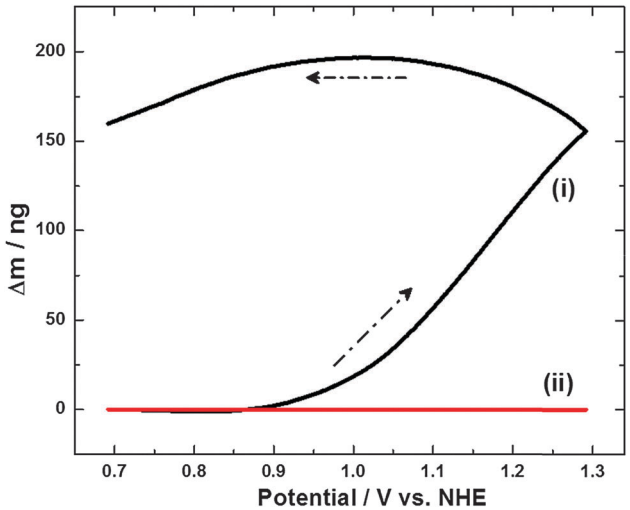

Fig. 2 Mass variations (Δ*m*) *vs.* potential of the Au-coated quartz crystal in 0.1 M neutral acetate solutions (i) containing 0.5 mM Co^{2+} and (ii) without Co^{2+}. The area of the electrode = 0.205 cm^2.

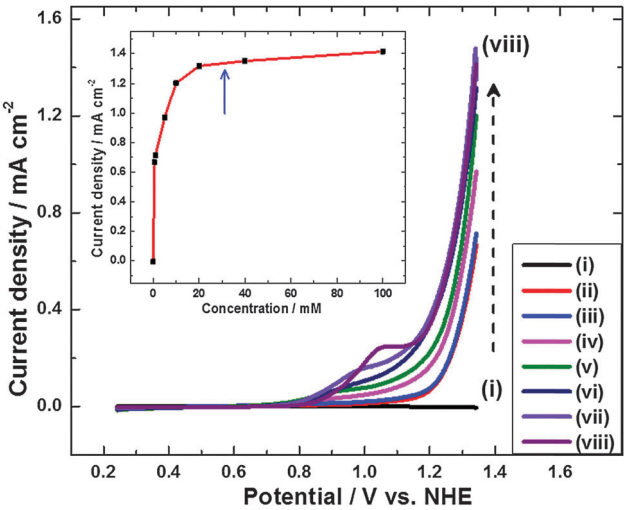

Fig. 3 Linear sweep voltammograms of the carbon paper electrode in 0.1 M acetate buffer (pH 7.0) containing (i) 0.0, (ii) 0.5, (iii) 1.0, (iv) 5.0, (v) 10, (vi) 20, (vii) 40 and (viii) 100 mM Co^{2+}. The inset shows variation in the current density at 1.34 V with Co^{2+} concentration.

sweep voltammetry (ESI,† Fig. S2). A current peak corresponding to the reduction of O_2 thus confirmed that the oxidation product at the Co–Ac electrode was O_2 only. It was also found that the OER current was independent of acetate ion concentration in the buffer solution (ESI,† Fig. S3).

The deposition of Co–Ac was quantitatively measured using EQCM. Fig. 2 shows variation in the mass of the Au electrode during cyclic voltammetry experiments in acetate solution in the presence (Fig. 2 curve i) and absence of Co^{2+} (Fig. 2 curve ii). There is no noticeable change in the mass of the electrode in the absence of Co^{2+} (Fig. 2 curve ii). However, there is a net mass gain of about 160 ng after completing one cycle in 0.1 M acetate containing 0.5 mM Co^{2+} (Fig. 2 curve i). There is no change in mass until the potential reaches 0.90 V, indicating the absence of any electrodeposition between 0.24 and 0.90 V. However, at 0.90 V, mass starts increasing and reaches 155 ng after completing the first anodic half cycle. On sweep reversal at 1.29 V, mass continues to increase rather slowly until the potential reaches back to 0.90 V. Further sweeping of potential below 0.90 V causes a partial reduction of the catalyst and hence a marginal decrease in the electrode mass. Thus, the net gain in mass after completing one potential cycle at 5 mV s^{-1} in 0.1 M acetate solution (pH 7.0) containing 0.5 mM Co^{2+} is about 160 ng. This quantitative measurement further confirms the electrodeposition of Co–Ac even at a low concentration of Co^{2+} ions in acetate solution. Additionally, the electrodeposition of the cobalt based OEC from acetate buffer is more interesting as the solubility of Co^{2+} in phosphate buffer solution is limited to 0.5 mM whereas it is more than 100 times in acetate buffer solution under identical experimental conditions.

The effect of concentration of Co^{2+} in acetate solution was investigated by conducting linear sweep voltammetry experiments at various Co^{2+} concentrations ranging from 0.5 to 100 mM and the results are shown in Fig. 3. At 1.34 V, current increases from 0.60 mA cm^{-2} in the 0.5 mM Co^{2+} electrolyte to about 1.50 mA cm^{-2} in 100 mM Co^{2+} solution. The anodic current peak at about 1.04 V corresponding to the formation of Co–Ac is clearly observed when the concentration of Co^{2+} is >40 mM (Fig. 3 curves vii and viii). The catalyst deposition starts at a potential as low as 0.84 V and the onset of OER occurs at 1.14 V. On sweep reversal at 1.34 V, broad current peaks are observed. The inset in Fig. 3 shows the variation of current at 1.34 V with Co^{2+} ion concentration. Initially, there is a rapid increase in current with the concentration of Co^{2+} up to 30 mM followed by a gradual increase. This could be due to the formation of thick and less conducting layers of the catalyst on the electrode surface at high concentrations. These results, thus, reveal that the Co-based OER catalyst (Co–Ac) can be electrodeposited from acetate electrolytes, similar to the formation of Co–Pi from phosphate electrolytes with additional advantages of higher solubility of Co^{2+}, formation of thicker layers of the catalyst and enhanced catalytic activity.

Growth of the Co–Ac catalyst on a carbon paper electrode was studied by bulk electrolysis in an acetate electrolyte (pH 7.0) at 1.24 V for 6 h (Fig. 4). In the absence of Co^{2+} in acetate solution (Fig. 4 curve i), current is negligibly small throughout the electrolysis. In the presence of 0.5 mM Co^{2+} (Fig. 4 curve ii), however, current increases initially rapidly and reaches a nearly steady value of 0.1 mA cm^{-2} in about 4 h. During this process, a steady growth of brownish Co–Ac catalyst was visually observed along with an increasing evolution of oxygen bubbles. The bulk electrolysis thus suggests the formation of the catalyst even at a concentration as low as 0.5 mM Co^{2+} in the acetate electrolyte. At the end of 6 h, the current value is about 0.13 mA cm^{-2}. Similar experiments at 5.0 (Fig. 4 curve iii) and 50 mM Co^{2+} (Fig. 4 curve iv) concentrations provide 0.20 and 0.35 mA cm^{-2}, respectively, after 6 h of electrolysis. Catalytic activity of the deposited Co–Ac was obvious from these experiments as there were no gas bubbles

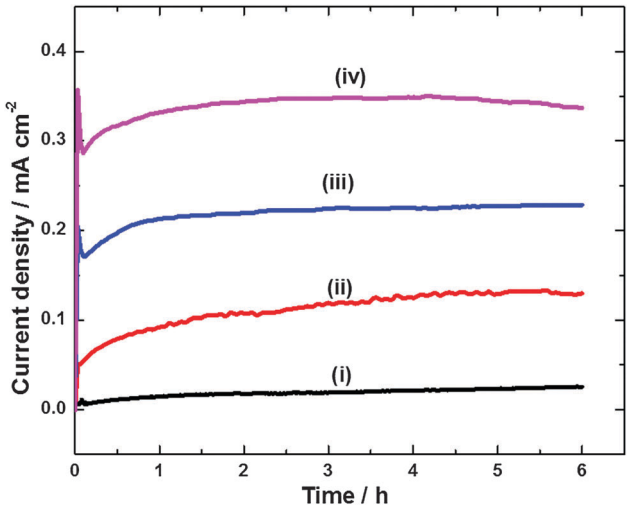

Fig. 4 Bulk electrolysis current at 1.24 V for 6 h using the carbon paper electrode in 0.1 M acetate buffer solution containing (i) 0.0, (ii) 0.5, (iii) 5.0 and (iv) 50 mM Co^{2+}.

noticed on the electrode surface in the initial stages of electrolysis and gas evolution became more and more vigorous with time as a thick layer of the catalyst was formed on the surface. In contrast, the presence of oxygen bubbles was not observed during any stage of electrolysis in the absence of Co^{2+} (Fig. 4 curve i).

To quantitatively monitor the Co–Ac deposition process during constant potential electrolysis at 1.19 V, mass variations of Au-coated quartz crystal electrodes were recorded *in situ* for different concentrations of Co^{2+} using EQCM (Fig. 5). The results show that the mass deposited after 5 min of electrolysis in 0.1 M acetate solution containing 0.5 mM Co^{2+} (Fig. 5 curve i) is 0.48 μg which is less than 0.68 μg obtained for 0.5 mM Co^{2+}

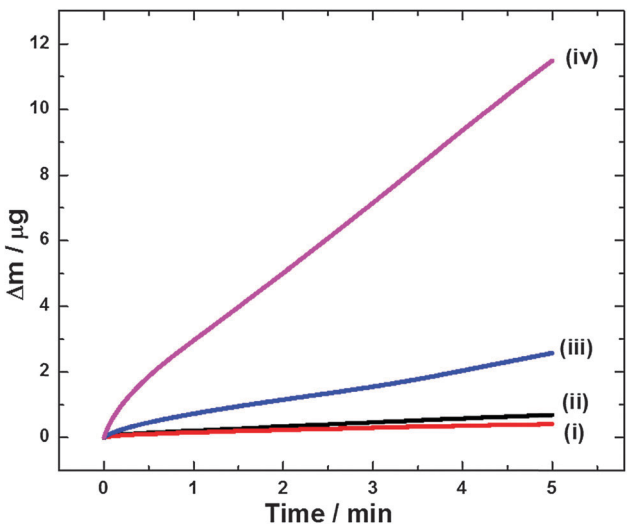

Fig. 5 Mass difference (Δ*m*) *vs.* time plot during the deposition of the Co–Ac catalyst on the Au electrode of area = 0.205 cm^2 at 1.19 V for 5 min from (i) 0.5 mM Co^{2+} in 0.1 M acetate, (ii) 0.5 mM Co^{2+} in 0.1 M phosphate, (iii) 5 mM Co^{2+} in 0.1 M acetate and (iv) 50 mM Co^{2+} in 0.1 M acetate electrolytes.

in 0.1 M phosphate solution (Fig. 5 curve ii). This could be due to the lower molar mass of the acetate ion than the phosphate ion. Nevertheless, the quantity of the Co–Ac catalyst deposited can be enhanced further by increasing the concentration of Co^{2+}, as the solubility of Co^{2+} salts is several times greater in acetate solution than in phosphate solution. This is readily observed by conducting similar experiments in acetate solutions containing 5 mM Co^{2+} (Fig. 5 curve iii) and 50 mM Co^{2+} (Fig. 5 curve iv), which resulted in a net mass of 2.57 and 11.48 μg, respectively, after 5 min. The average values of the rate of electrodeposition of Co–Ac are 5.8, 37.5 and 175 ng cm^{-2} s^{-1}, respectively, for Co^{2+} concentrations of 0.5, 5 and 50 mM (Fig. 5 curves i, ii and iv). The corresponding value for Co–Pi (Fig. 5 curve ii) in phosphate buffer solution containing 0.5 mM Co^{2+} is only 10.4 ng cm^{-2} s^{-1}. These quantitative investigations further throw light on the importance of electrodeposition of the Co–Ac catalyst for oxygen evolution.

3.2 Oxygen evolution reaction kinetics

To study the effect of thickness of the catalyst layer on the kinetic of OER, Co–Ac was deposited in various thicknesses on carbon paper electrodes from 50 mM Co^{2+} in 0.1 M acetate solution by passing charge in the range from 50 to 400 mC cm^{-2}. The electrodes were washed with double-distilled water and dried at 70 °C in vacuum. Catalytic activity was studied by linear sweep voltammetry at 0.05 mV s^{-1} in the phosphate electrolyte (pH 7.0) under stirring conditions (Fig. 6a). Phosphate buffer solution was used because Co–Ac exhibits greater activity in the phosphate electrolyte than in the acetate electrolyte of the same pH as discussed below. The values of current density measured at 1.39 V are 0.21, 0.37, 0.83, 1.52, 1.87 and 2.38 mA cm^{-2}, respectively, for the Co–Ac catalyst prepared by passing 50, 75, 100, 200, 300 and 400 mC cm^{-2} (Fig. 6a curves i–vi). Thus, the results show that the catalytic activity of Co–Ac increases with an increase in the catalyst loading. The enhancement in the OER activity with increasing thickness of Co–Ac film is attributed to an increase in the density of surface active sites, which facilitate adsorption of OH. In neutral and alkaline electrolytes, OER is written as,

$$4OH^- \rightleftharpoons 2H_2O + O_2 + 4e^- \quad (1)$$

with a reversible electrode potential (E^r) of 0.81 V at pH 7.0. The generally accepted mechanism for OER[24–27] is as follows.

$$S + OH^- \rightleftharpoons S\text{–}OH + e^- \quad (2)$$

$$S\text{–}OH + OH^- \rightleftharpoons S{=}O + H_2O + e^- \quad (3)$$

$$2S{=}O \rightleftharpoons 2S + O_2 \quad (4)$$

where S is the substrate site, which facilitates adsorption of OH species. The oxidation of OH^- ion is a single electron transfer step resulting in the formation of adsorbed OH as shown in reaction (2). Reaction (3) involves another single electron transfer producing adsorbed O. Oxygen evolution takes place chemically by combination of these adsorbed O atoms on adjacent sites as in step (4). The current density (i) and potential

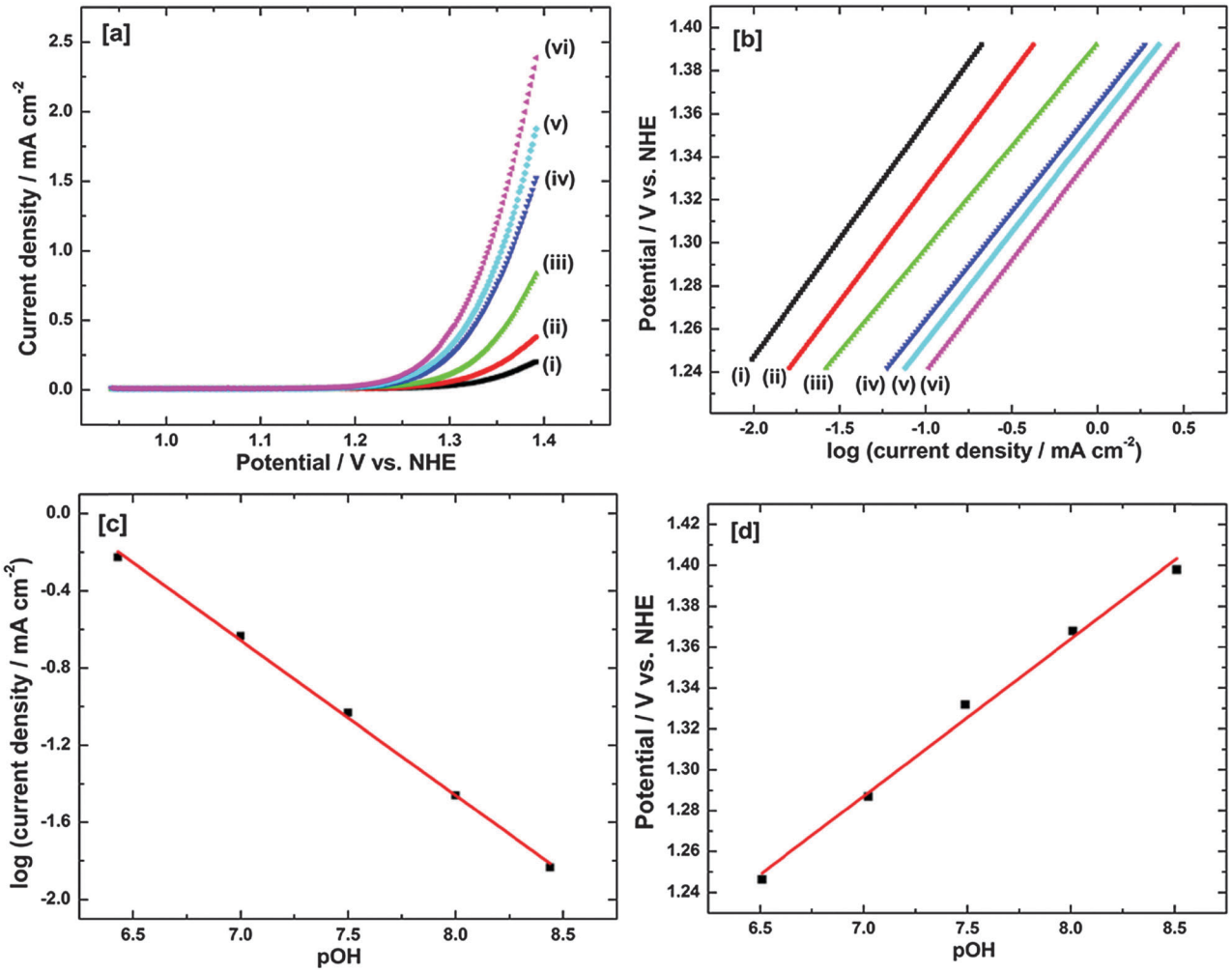

Fig. 6 (a) Linear sweep voltammograms of the Co–Ac catalyst prepared using (i) 50, (ii) 75, (iii) 100, (iv) 200, (v) 300 and (vi) 400 mC cm^{-2} on carbon paper in phosphate buffer solution of pH 7.0. Scan rate: 0.05 mV s^{-1}, (b) the corresponding Tafel plots, (c) p^{OH} dependence of steady state current density at 1.29 V and (d) p^{OH} dependence of steady-state electrode potential at 50 μA cm^{-2}. Data in (c) and (d) are measured at the Co–Ac catalyst prepared using 50 mC cm^{-2}.

(E) relationship of the electron-transfer controlled step of OER may be written as

$$i = i_0(1 - \theta)\exp[(1 - \alpha)nF(E - E^r)]/(RT) \quad (5)$$

where i_0 is the exchange current density, θ is the surface coverage by adsorbed species, $(1 - \alpha)$ is the transfer coefficient and other symbols have their usual meanings. If either step (2) or step (3) is considered as the rate determining step, assuming θ is constant, the Tafel slope ($dE/d\log i$) becomes,

$$(dE/d\log i) = 2.3RT/[(1 - \alpha)F] \quad (6)$$

$$= 0.059/(1 - \alpha)\ \text{V at 25 °C} \quad (7)$$

Assuming a symmetrical energy barrier (*i.e.*, $\alpha = 0.5$), the value of the Tafel slope is expected to be 118 mV. Tafel data of OER measured on the Co–Ac catalyst of various thicknesses are shown in Fig. 6b. The values of the Tafel slope are 105, 106, 100, 101, 102 and 103 mV decade^{-1}, respectively, for Co–Ac catalysts prepared using charge 50, 75, 100, 200, 300 and 400 mC cm^{-2}. The average value of Tafel slopes thus becomes 103 ± 3 mV decade^{-1}. Dependence of Co–Ac catalyst thickness on the Tafel slope is not observed. This value is comparable to 100 mV decade^{-1} reported for OER in the phosphate electrolyte at the Co–Pi catalyst deposited FTO-coated glass electrode.[12]

The reaction order with respect to OH^- activity was measured from constant potential electrolysis at 1.29 V using the Co–Ac catalyst (prepared using 50 mC cm^{-2}) in the 0.1 M phosphate electrolyte by gradually increasing p^{OH} of the solution from 6.50 to 8.50. The electrolysis was carried out for 5 min at each p^H to ensure a steady value of current. A plot of log(current density) *vs.* p^{OH} (Fig. 6c) results in a straight line with a slope of 0.79. Additionally, the p^{OH} dependence of water oxidation is studied using the galvanostatic titration method. For this, a constant current density of 50 μA cm^{-2} was applied and the corresponding potential was measured while the p^{OH} was gradually increased from 6.5 to 8.5 (Fig. 6d). A linear fit of the data in Fig. 6d yields a slope of 78 mV. The Tafel slope (Fig. 6b) can be

correlated with the slopes of potential *vs.* p^{OH} (Fig. 6d) and log(current density) *vs.* p^{OH} (Fig. 6c) plots using the following equation,[21]

$$(\partial E/\partial p^{OH})_i = (\partial E/\partial \log(i))_{p^{OH}} (\partial \log(i)/\partial p^{OH})_E \quad (8)$$

From the values of 0.79 and 78 mV of $(\partial \log(i)/\partial p^{OH})_E$ and $(\partial E/\partial p^{OH})_i$, respectively, the value of $(\partial E/\partial \log(i))_{p^{OH}}$ is calculated to be 99 mV. This value is in agreement with the value of the average Tafel slope (103 mV decade^{-1}) obtained as above from Fig. 6b. Thus, it is inferred that a single electron transfer reaction, *i.e.*, either reaction (2) or reaction (3) is the rate determining step of reaction (1). Using the value of 103 mV decade^{-1} for the Tafel slope, the value of α, thus, becomes 0.43. As it is known that reaction (2) is the rate determining step on Pt-based catalysts,[28] reaction (2) is anticipated as the rate determining step on the Co–Ac catalyst also.

3.3 Synergistic effect of phosphate buffer solution on the catalytic activity of Co–Ac

It was intended to investigate the catalytic activity of Co–Ac in phosphate and acetate buffer electrolytes in the absence of Co^{2+}. For this, a layer of Co–Ac was deposited on the carbon paper electrode at 1.29 V for 1 h from acetate (pH 7.0) containing 0.5 mM Co^{2+}. The electrode was washed with double-distilled water and dried in vacuum. The electrode, without any pre-treatment, was then transferred to the phosphate or acetate electrolyte under study. Linear sweep voltammograms were recorded at 0.05 mV s^{-1} both in phosphate (Fig. 7 curve i) and acetate (Fig. 7 curve ii) electrolytes. The current density values at 1.34 V are about 0.45 and 0.25 mA cm^{-2}, respectively, in phosphate and acetate electrolytes. Thus, Co–Ac shows almost twice OER activity in phosphate buffer in comparison with the acetate electrolyte.

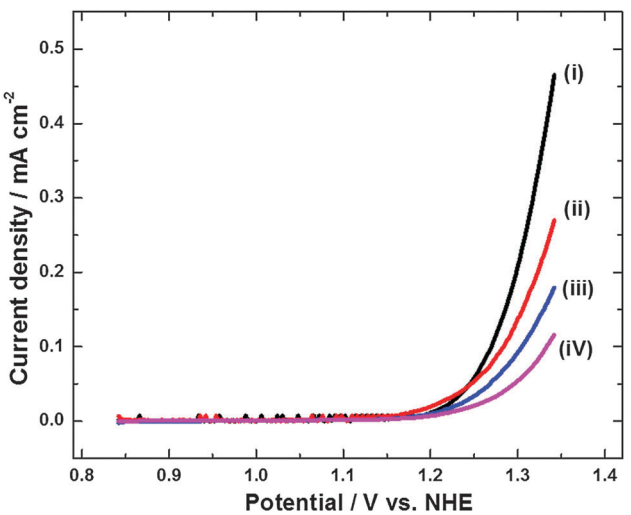

Fig. 7 Linear sweep voltammograms of the Co–Ac catalyst deposited carbon paper electrode in (i) phosphate, (ii) acetate electrolytes and Co–Pi deposited carbon paper in (iii) acetate and (iv) phosphate electrolytes. Sweep rate: 0.05 mV s^{-1}. The catalyst was deposited from 0.5 mM Co^{2+} at 1.29 V for 1 h.

To compare the activity of Co–Ac with the Co–Pi catalyst, experiments were also conducted with the Co–Pi coated carbon paper electrode. Co–Pi deposition was carried out in 0.5 mM Co^{2+} ion concentration in the phosphate buffer electrolyte. Interestingly, the Co–Pi catalyst exhibits greater current in the acetate electrolyte (Fig. 7 curve iii) than in the phosphate electrolyte (Fig. 7 curve iv). Thus, there are three interesting observations: (1) OER activity of Co–Ac (Fig. 7 curves i and ii) is much superior to that of Co–Pi (Fig. 7 curves iii and iv) both in terms of onset potential and current density at any potential in the OER region. This observation is valid for both the buffer electrolytes used, (2) the catalytic activity of Co–Ac is almost twice in phosphate buffer than in acetate buffer of the same pH and (3) the activity of Co–Pi is greater in the acetate electrolyte than in the phosphate electrolyte.

The Co–Ac catalyst in the phosphate electrolyte exhibits the highest OER catalytic activity. From the elemental analysis as detailed below, the presence of both phosphate and acetate in Co–Ac used for electrolysis in phosphate buffer solution and also in Co–Pi used for electrolysis in acetate buffer solution is observed. Thus, it is observed that there is a partial exchange of acetate present in the Co–Ac catalyst with phosphate of the electrolyte. This results in the formation of a hybrid Co–Ac–Pi catalyst. Similarly, when Co–Pi is used in acetate solution, a partial exchange of phosphate present in the Co–Pi catalyst with acetate of the electrolyte results in the formation of Co–Ac–Pi. The Co–Ac–Pi catalyst so formed either from Co–Ac or Co–Pi exhibits greater activity towards oxygen evolution in relation to the pristine catalysts. The Co–Ac–Pi formed from Co–Ac exhibits the highest activity. Therefore, it is proposed that there is a synergistic effect of acetate and phosphate ions on the activity of the Co catalyst. The electrochemical stability of the Co–Ac catalyst in phosphate buffer solution was examined by continuous electrolysis at 1.34 V for 24 h (ESI,† Fig. S4). Current is nearly constant during the entire period of electrolysis. Thus, the stability of the catalyst is ensured.

Morphology of the Co–Ac electrocatalyst was examined using SEM. Fig. 8a and b show the morphology of the Co–Ac catalyst deposited on the ITO coated glass electrode at 1.29 V for 2 h from 50 mM Co^{2+} + acetate solution at different magnifications. Cracks are observed (Fig. 8a) on the dried sample similar to Co–Pi deposited on the FTO electrode.[11] The islands formed in between the cracks have an irregular shape with sizes ranging from 15 to 30 μm. A higher magnification image (Fig. 8b) of the electrode indicates that the Co–Ac catalyst comprises of spherical particles of diameter in the range from 200 nm to 2 μm. A few larger size globules are also seen. Furthermore, SEM micrographs were recorded after 6 h of electrolysis at 1.29 V both in phosphate (Fig. 8c and d) and acetate (Fig. 8e and f) electrolytes. In both the cases, the catalyst layers are broken down into numerous tiny islands (Fig. 8c and e). The shape of tiny islands formed in the phosphate electrolyte (Fig. 8c) resembles the shape of pristine catalyst islands (Fig. 8a), but with size smaller by about 10 times. Interestingly, the inner-layer of the electrode observed at a higher magnification (Fig. 8d) is smooth with islands separated

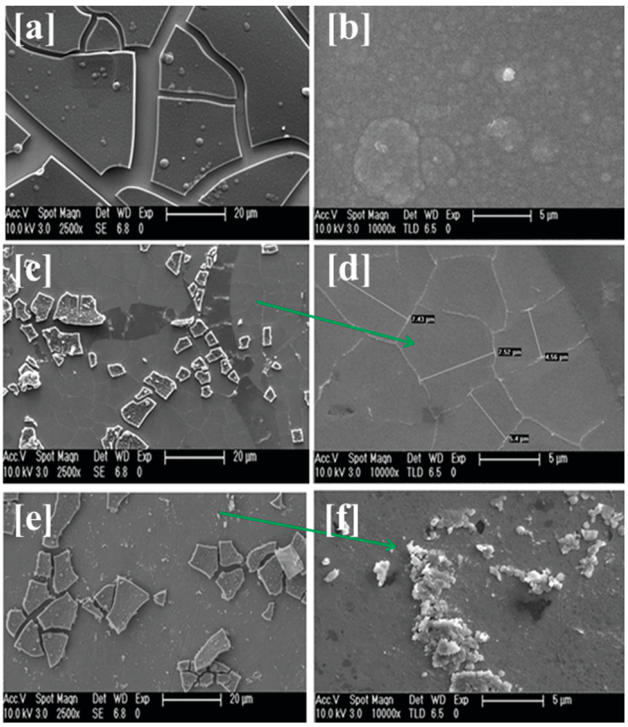

Fig. 8 SEM micrographs of Co–Ac electrodeposited on the ITO coated glass electrode (1 cm^2) at 1.29 V for 2 h from 50 mM Co^{2+} + acetate buffer solution (pH 7.0) at (a) 2500× and (b) 10 000×. SEM images of the similar electrodes after electrolysis at 1.29 V for 6 h in phosphate buffer solution (pH 7.0) at (c) 2500× and (d) 10 000×. Similar micrographs after electrolysis at 1.29 V for 6 h in acetate buffer solution (pH 7.0) at (e) 2500× and (f) 10 000×.

by boundaries but not by cracks as observed in Fig. 8a. It is anticipated that the formation of this layer could be due to the partial dissolution of the as-deposited Co–Ac from the electrode surface and its subsequent re-deposition as Co–Pi, resulting in the formation of the Co–Ac–Pi catalyst layer. Dissolution and re-deposition of the Co–Pi is well discussed as a self-healing mechanism.[19] A similar phenomenon is expected to occur for Co–Ac also. Development of Co–Ac–Pi additional catalytic regions may be responsible for the enhanced activity of Co–Ac in phosphate than in the acetate electrolyte. After electrolysis in acetate solution also (Fig. 8e), Co–Ac electrodes break down and smaller islands are formed on the outer layer. But the morphology of the inner layer (Fig. 8f) indicates the presence of an ill-defined shape or a spongy-type particle without any clear inter-particulate separation (Fig. 8e and f). Thus, the composition of the electrolyte influences the morphology of Co–Ac catalyst layers.

Powder XRD patterns were recorded for the bare carbon paper substrate and for the Co–Ac catalyst deposited (35 C cm^{-2}) on carbon paper (ESI,† Fig. S5). The pattern for the substrate consisted of peaks at 2θ = 26.2 and 54.4° due to carbon crystallites. Only these reflections were identified even after the catalyst deposition, thus reflecting the amorphous nature of the Co–Ac catalyst. The composition of the electrodeposited material was further analysed by EDXA and XPS. Energy-dispersive X-ray analysis (EDXA) spectra were obtained from multiple regions of Co–Ac samples before and after electrolysis in the phosphate electrolyte. Results are shown in Fig. 9. The ratio of Co : C : O in the as prepared Co–Ac sample is approximately 1 : 1 : 2 (Fig. 9a). Unlike in the case of Co–Pi,[11] the amount of Na present in the Co–Ac catalyst layer is negligibly small. Interestingly, P and K are also present in the Co–Ac film after 6 h of electrolysis in the phosphate buffer electrolyte (Fig. 9b and c). However, there is a significant difference in the chemical composition of top (Fig. 9b) and bottom layers (Fig. 9c) corresponding to the SEM micrographs of Co–Ac (Fig. 8c and d) after electrolysis in phosphate buffer. For the top layer (Fig. 9b), the Co : C : O ratio is changed to 1 : 1 : 2.65 from 1 : 1 : 2 as observed in the as-deposited Co–Ac. Increase in the percentage of oxygen and the presence of K and P suggest the addition of PO_4^{3-} from the electrolyte. However, the bottom layer (Fig. 9c) exhibits a Co : P ratio of 1 : 1.8 similar to Co–Pi deposited on the Au-electrode[29] and a relatively high Co : O ratio (1 : 10). Therefore, it is anticipated that the bottom layer is converted into Co–Pi rather than being present as Co–Ac. The presence of this additional layer in the SEM images together with detection of P and K in the EDXA spectrum suggests the formation of the Co–Pi layer in the cracks developed during electrolysis.

For XPS analysis, Co–Ac was deposited (20 C cm^{-2}) on carbon paper from 50 mM Co^{2+} in acetate buffer solution (pH 7.0). The spectra are shown in Fig. 10. The survey spectrum (Fig. 10a) identifies Co, C and O in the Co–Ac deposit which is in agreement with EDXA results. In the Co region (Fig. 10b), two peaks are identified with binding energies of 796.1 eV and 780.9 eV corresponding to Co $2p_{1/2}$ and Co $2p_{3/2}$,[30] respectively. Furthermore, additional satellite peaks are observed in the vicinity of the Co $2p_{3/2}$ line. It is known that all Co(II) compounds are high spin paramagnetic complexes (s = 3/2) whereas the low spin Co(III) complexes are diamagnetic (s = 0).[30] As a consequence, Co(II) compounds show intense broad shake-up peaks at higher binding energies. Such additional peaks are either weak or absent in the case of diamagnetic Co(III) complexes.[31,32] In the present case, relatively sharper Co 2p main peaks (Fig. 10b) along with broad additional shake-up features are indicative of the presence of both Co(II) and Co(III) states. It is expected that the Co(II)/Co(III) ratio is not much significant in OER activity of the catalyst because oxidation states of Co in the catalyst change continuously [Co(II) → Co(III)/Co(IV) → Co(II)] in a cyclic manner during the course of oxygen evolution similar to Co–Pi.[33] It was further intended to study the effect of electrolysis in phosphate buffer solution. For this, Co–Ac was deposited on the carbon paper electrode and subjected to electrolysis at 1.29 V for 3 h in phosphate solution, washed and dried before recording XPS. The survey spectrum (Fig. 10c) is similar to that of as deposited Co–Ac (Fig. 10a) but with additional peaks corresponding to K and P. This supports SEM and EDXA results that Co–Pi under layers are formed after OER catalysis in phosphate buffer. Moreover, binding energy values of the peaks in the Co 2p spectra (Fig. 10d) are slightly shifted to lower values (795.7 eV and 780.5 eV) indicating a direct interaction of phosphate species with Co-centres. The high resolution P 2p

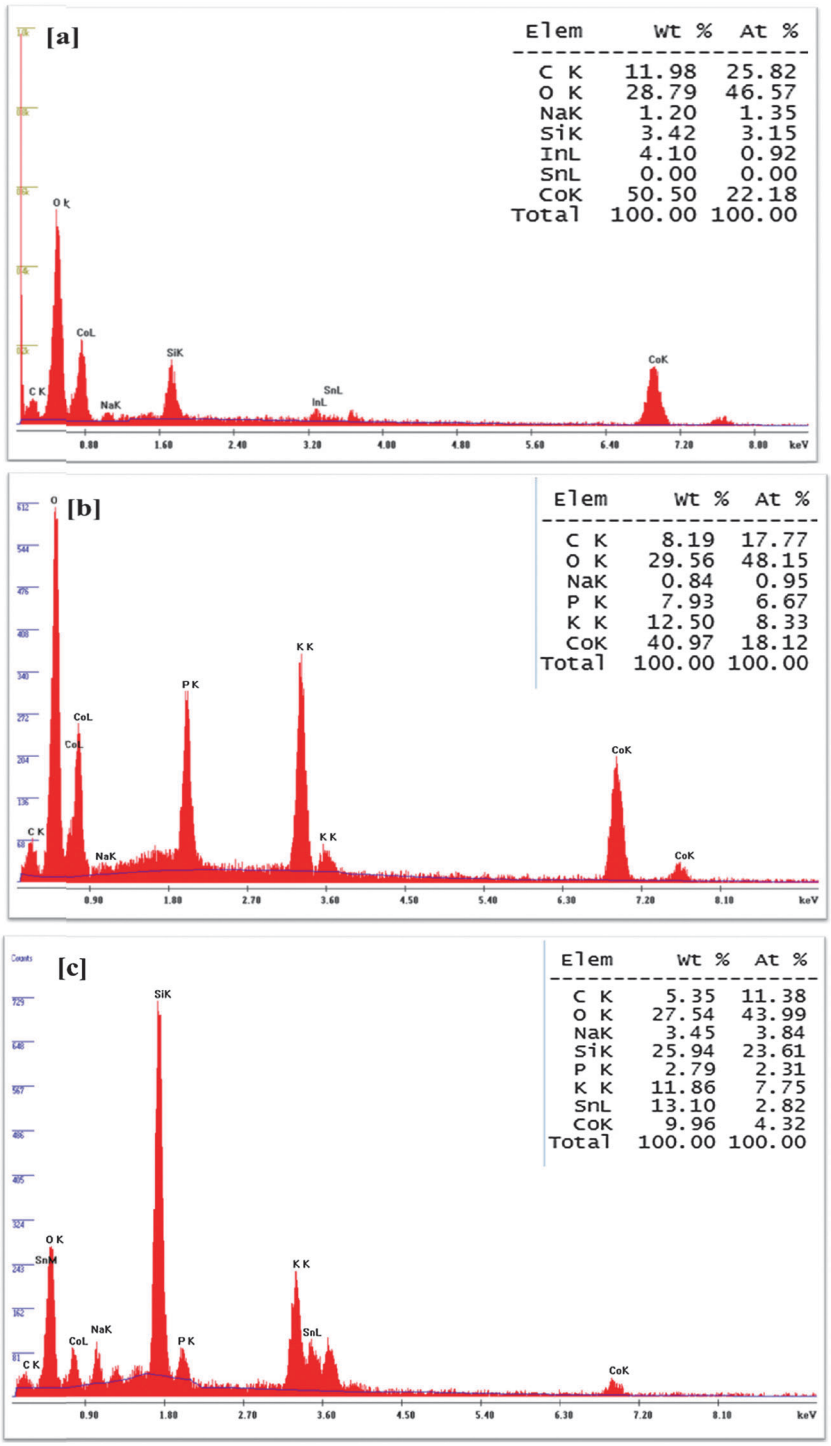

Fig. 9 EDXA analysis for Co–Ac deposited on the ITO coated glass electrode at 1.29 V for 2 h from 50 mM Co^{2+} in 0.1 M acetate solution (a) before electrolysis and (b, c) after electrolysis at 1.29 V for 6 h in phosphate buffer solution, (b) for the top layer region and (c) for the bottom layer region.

peak (Fig. 10e) at 132.8 eV is ascribed to phosphate in the Co–Pi layer as reported in the case of electrodeposited Co–Pi on the FTO coated glass electrode.[11,33] These observations support that the Co–Ac catalyst is converted into a more active Co–Ac–Pi catalyst by using the phosphate electrolyte for OER.

The molecular structure of the Co–Ac catalyst was analysed by recording the IR spectrum. For this, Co–Ac was deposited on a large ITO coated glass electrode at 1.29 V from 0.1 M acetate buffer containing 50 mM Co^{2+}. The electrode was dried at 100 °C for 3 h under vacuum and the material was scrapped off using a razor blade. The IR-spectrum of the as-deposited material in the 400–4000 cm^{-1} region (Fig. 11) is characterized by a pair of peaks at 1411 and 1559 cm^{-1}. These peaks with a separation of 148 cm^{-1} are attributed to the antisymmetric

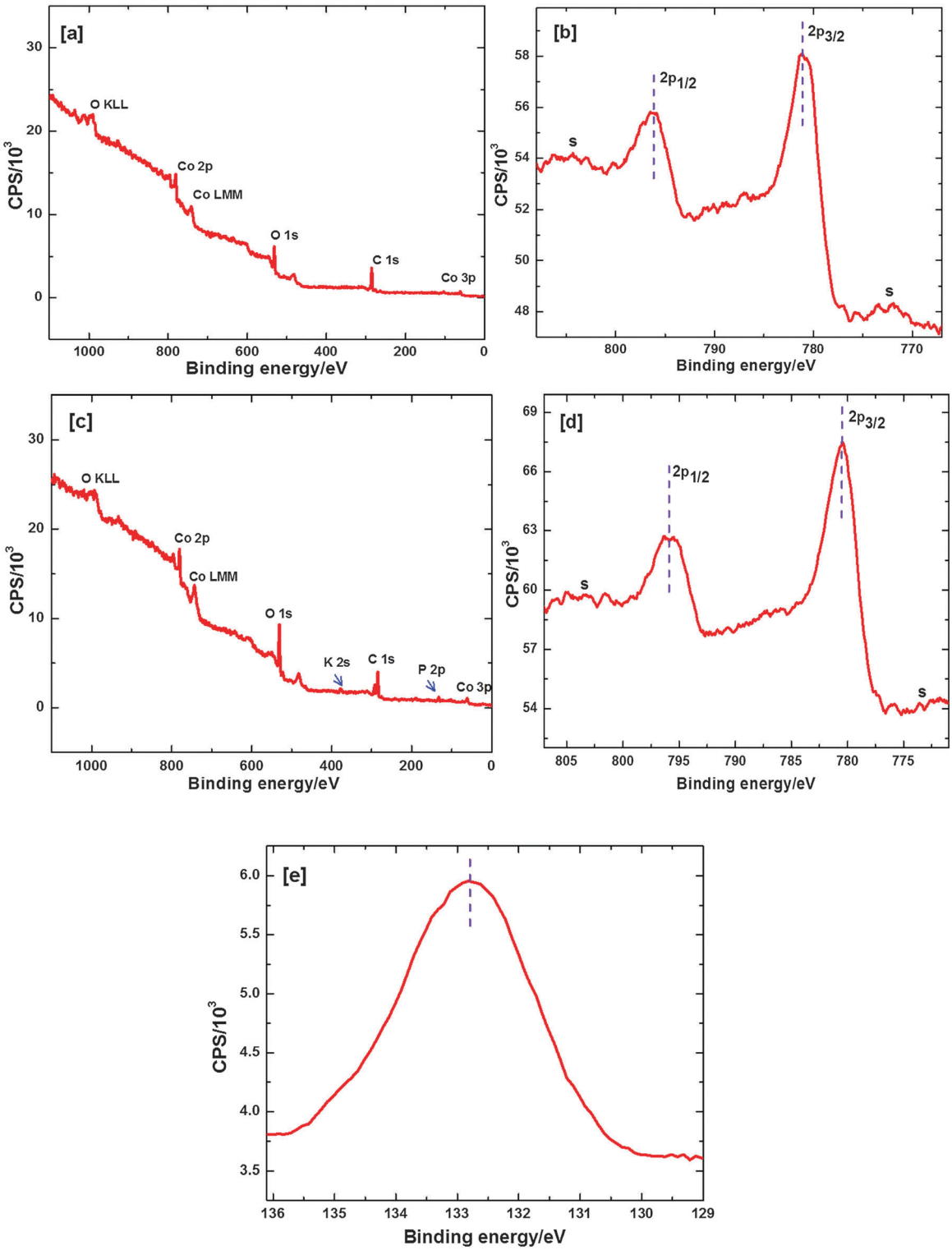

Fig. 10 XPS spectra of the electrodeposited Co–Ac film (20 C cm^{-2}) on carbon paper. (a and b) before electrolysis and (c to e) after 3 h of electrolysis at 1.29 V in phosphate buffer solution (pH 7.0). Here, (a and c) survey spectrum, (b and d) Co 2p and (e) P 2p detailed spectra.

stretching and symmetric stretching, vibrations of the free acetate ion,[34] respectively. The acetate anion can coordinate to Co in three ways, *i.e.*, monodentate, bidentate chelating and bidentate bridging, and their stretching frequencies differ according to their coordination.[35] However, in the as-prepared Co–Ac, acetate ions are likely to exist as un-coordinated in analogy with phosphate in Co–Pi.[36] Recent EXAFS investigation on Co–Pi[36] suggests that there is no extensive bonding between

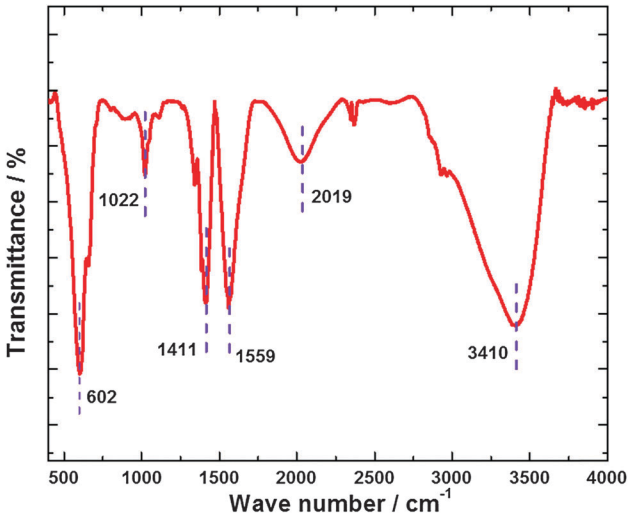

Fig. 11 Infra-red spectrum of the electrochemically prepared Co–Ac catalyst on the ITO coated glass electrode. Samples are diluted using KBr.

cobalt and phosphate. Thus, phosphate ions are mobile within Co–Pi which is considered to have layered-double-hydroxide like structure.[37] Similarly, Co–Ac is expected to have charged layers of Co-hydroxide/oxyhydroxide, which accommodate free acetate ions in the interlayer region.

4. Conclusions

The high catalytic activity of electrochemically deposited Co–Ac towards OER was demonstrated. Acetate buffer solution was employed for *in situ* deposition of Co-OEC because of greater solubility of Co^{2+} salts in comparison with widely studied phosphate buffer solution. When the Co–Ac catalyst was used for electrolysis in phosphate solution, formation of a hybrid Co–Pi–Ac was observed, which resulted in greater catalytic activity owing to the synergistic effect of phosphate ions in the catalyst layer.

Acknowledgements

The authors thank Aneesh Joesph and Dr Ambily Mathew for their help in physical characterization.

References

1 D. Abbott, *Proc. IEEE*, 2010, **98**, 42–66.
2 M. I. Hoffert, K. Caldeira, A. K. Jain, E. F. Haites, L. D. D. Harvey, S. D. Potter, M. E. Schlesinger, S. H. Schneider, R. G. Watts, T. M. L. Wigley and D. J. Wuebbles, *Nature*, 1998, **395**, 881–884.
3 D. G. Nocera, *Chem. Soc. Rev.*, 2009, **38**, 13–15.
4 N. S Lewis and D. G. Nocera, *Proc. Natl. Acad. Sci. U. S. A.*, 2006, **103**, 15729–15735.
5 J. L. Dempsey, A. J. Esswein, D. R. Manke, J. Rosenthal, J. D. Soper and D. G. Nocera, *Inorg. Chem.*, 2005, **44**, 6879–6892.
6 M. S. Wrighton, *Acc. Chem. Res.*, 1979, **12**, 303–310.
7 A. J. Bard and M. A. Fox, *Acc. Chem. Res.*, 1995, **28**, 141–145.
8 R. Eisenberg and H. B. Gray, *Inorg. Chem.*, 2008, **47**, 1697–1699.
9 T. A. Betley, Q. Wu, T. V. Voorhis and D. G. Nocera, *Inorg. Chem.*, 2008, **47**, 1849–1861.
10 M. Gratzel, *Nature*, 2001, **414**, 338–344.
11 M. W. Kanan and D. G. Nocera, *Science*, 2008, **321**, 1072–1075.
12 E. R. Young, D. G. Nocera and V. Bulovic, *Energy Environ. Sci.*, 2010, **3**, 1726–1728.
13 E. R. Young, R. Costi, S. Paydavosi, D. G. Nocera and V. Bulovic, *Energy Environ. Sci.*, 2011, **4**, 2058–2061.
14 E. M. P. Steinmiller and K. S. Choi, *Proc. Natl. Acad. Sci. U. S. A.*, 2009, **106**, 20633–20636.
15 R. S. Khnayzer, M. W. Mara, J. Huang, M. L. Shelby, L. X. Chen and F. X. Castellano, *ACS Catal.*, 2012, **2**, 2150–2160.
16 J. A. Seabold and K. S. Choi, *Chem. Mater*, 2011, **23**, 1105–1112.
17 D. K. Zhong, J. Sun, H. Inumaru and D. R. Gamelin, *J. Am. Chem. Soc.*, 2009, **131**, 6086–6087.
18 D. K. Zhong, M. Cornuz, K. Sivula, M. Gratzel and D. R. Gamelin, *Energy Environ. Sci.*, 2011, **4**, 1759–1764.
19 D. K. Zhong and D. R. Gamelin, *J. Am. Chem. Soc.*, 2010, **132**, 4202–4207.
20 S. K. Pilli, T. E. Furtak, L. D. Brown, T. G. Deutsch, J. A. Turnerc and A. M. Herring, *Energy Environ. Sci.*, 2011, **4**, 5028–5034.
21 Y. Surendranath, M. W. Kanan and D. G. Nocera, *J. Am. Chem. Soc.*, 2010, **132**, 16501–16509.
22 Y. Surendranath, M. Dinca and D. G. Nocera, *J. Am. Chem. Soc.*, 2009, **131**, 2615–2620.
23 I. Zaharieva, P. Cherenev, M. Risch, K. Klingan, M. Kohlhoff, A. Fischer and H. Dau, *Energy Environ. Sci.*, 2012, **5**, 7081–7089.
24 M. E. G. Lyons and M. P. Brandon, *Int. J. Electrochem. Sci.*, 2008, **3**, 1386–1424.
25 Y. Matsumoto, H. Manabe and E. Sato, *J. Electrochem. Soc.*, 1980, **127**, 811–814.
26 P. Rasiyah and A. C. C. Tseung, *J. Electrochem. Soc.*, 1983, **130**, 2384–2386.
27 J. O'M. Bockris, *J. Chem. Phys.*, 1956, **24**, 81–827.
28 C. Iwakura, K. Fukuda and H. Tamura, *Electrochim. Acta*, 1976, **21**, 501–508.
29 A. Irshad and N. Munichandraiah, *J. Phys. Chem. C*, 2013, **117**, 8001–8008.
30 I. G. Casella and M. R. Guascito, *J. Electroanal. Chem.*, 1999, **476**, 54–63.
31 D. Briggs and V. A. Gibson, *Chem. Phys. Lett.*, 1974, **25**, 493–496.

32 K. J. McDonald and K. S. Choi, *Chem. Mater.*, 2011, **23**, 1686–1693.
33 S. Cobo, J. Heidkamp, P. A. Jacques, J. Fize, V. Fourmond, L. Guetaz, J. Bruno, V. Ivanova, H. Dau, S. Palacin, M. Fontecave and V. A. Artero, *Nat. Mater.*, 2012, **11**, 802–807.
34 Y. Zhu, H. Li, Y. Koltypin and A. Gedanken, *J. Mater. Chem.*, 2002, **12**, 729–733.
35 S. Doeuff, M. Henry, C. Sanchez and J. Livage, *J. Non-Cryst. Solids*, 1987, **89**, 206–216.
36 M. W. Kanan, J. Yano, Y. Surendranath, M. Dinca, V. K. Yachandra and D. G. Nocera, *J. Am. Chem. Soc.*, 2010, **132**, 13692–13701.
37 S. J. Harley, H. E. Mason, J. G. McAlpin, R. D. Britt and W. H. A. Casey, *Chem.–Eur. J.*, 2012, **18**, 10476–10479.